(Received 5 March 2025, Accepted 16 April 2025, Scheduled 21 June 2025)

Compact Dual-Band Wearable Antenna for Millimeter-Wave Applications: Designed for Medical and IoT Device Integration

Abubakar Salisu[1, 2, *], Umar Musa[3], Umar U. Sabo[4], Mustapha M. Abubakar[2], Abubakar S. Hussaini[5], Mobayode O. Akinsolu[6], Chan H. See[7], and Raed A. Abd-Alhameed[1, 8]

[1]*Department of Electronics and Biomedical Engineering, University of Bradford, United Kingdom*
[2]*Department of Electrical and Electronics Engineering, MAU Yola, Nigeria*
[3]*Department of Electrical Engineering, Bayero University Kano, 700006, Nigeria*
[4]*Electrical and Computer Technology Department, Gombe state Polytechnics Bajoga, Gombe*
[5]*School of Engineering, AUN Yola, Nigeria*
[6]*Faculty of Arts, Computing and Engineering, Wrexham University, Wales, UK*
[7]*School of Computing, Engineering and the Built Environment, Edinburgh Napier University, UK*
[8]*Department of Information and Communications Engineering, Al-Farqadein University College, Basrah 61004, Iraq*

ABSTRACT: This paper introduces a compact dual-band wearable antenna designed for mmWave applications. The antenna is fabricated on a Rogers 3003 semi-flexible substrate with dimensions of $15 \times 15 \times 1.52\,\text{mm}^3$ and features a circular radiating patch with a full ground plane. Initially designed to resonate at 28 GHz, the antenna incorporates a square split-ring resonator in the ground plane to achieve an additional resonance at 38 GHz. To improve bandwidth and gain, a round necktie configuration is applied by adding two diagonal rectangular patches to the periphery of the radiating patch. The measured impedance bandwidths are 21.4% at 28 GHz and 23.7% at 38 GHz. The antenna achieves gains of 5.91 dBi and 4.57 dBi, with efficiencies of 90% and 78% at the respective operating bands. Simulated SAR values are 0.57 W/kg and 0.31 W/kg for 1 g and 10 g of human tissue at 28 GHz, and 0.18 W/kg and 0.16 W/kg at 38 GHz. These SAR values comply with FCC and ICNIRP safety standards. Additionally, bending tests illustrate that the antenna's performance was stable under deformation. As a result, the proposed antenna is ideal for fast connectivity 5G and biomedical applications since it efficiently spans fundamental mmWave frequency ranges.

1. INTRODUCTION

Considering the goal of attaining greater data rates and a broader bandwidth, 5G wireless communication has become the subject of intensive study over the past decade [1, 2]. Among the many benefits of this approach are its capacity to produce compact wireless gadgets, lower latency, and improved reliability [3, 4]. In order to facilitate 5G deployment, the Federal Communications Commission (FCC) has identified certain frequency ranges between 3 and 300 GHz, which experts have broken down into two groups: sub-6 GHz and millimeter wave (mmWave) band 24 GHz and above [5–7]. The intricate nature of the design procedure is increased when developing antennas for 5G mmWave communications because of the need to carefully evaluate several elements, which includes bandwidth, gain, radiation characteristics, dimensions, and difficulties including atmospheric attenuation [8–10]. Furthermore, considering the widespread application in cutting-edge 5G communication systems, the mmWave spectrum is a crucial range of frequencies to investigate in the years to come [11]. Moreover, wearable antennas are crucial to body-worn devices because they transmit and receive information between body-worn devices and integrated devices. Thus, effectiveness could be potentially affected, unlike with off-body antennas. The primary cause for that is lossy and uneven contact with the human body [12–14]. Considering the human body functions primarily as a barrier that prevents radio frequencies from traveling through it, antenna optimization is crucial to maximizing efficiency. The body absorbs a large portion of these waves and transforms them into thermal energy [15–17]. Furthermore, it is crucial to examine how antennas affect tissue in humans, which can be evaluated by taking the specific absorption rate (SAR) limits into consideration. The rules of both the FCC and International Commission on Non-Ionizing Radiation Protection (ICNIRP) require adherence to these limitations [18–20]. At the same time, care must be taken when it comes to the antenna's size, trying to keep it as small as feasible [21]. Hence, wearable antenna for 5G wireless communication design has been considered a challenging undertaking. Several papers analyze the performance and design of mmWave antennas for numerous applications. A 25.5/38 GHz patch antenna has been found to be compatible with internet of things (IoT) applications in [22]. A coplanar waveguide-fed patch with a matching strip operating at 28/39 GHz is presented in [23]. Slot-based and coaxial-fed rectangular patch antennas operate at 33.5/60.8 GHz and are tested for body placement in medical IoT applications [24]. Four-element array antennas for high-gain mmWave applications covering bands between

* Corresponding author: Abubakar Salisu (a.salisu@bradford.ac.uk).

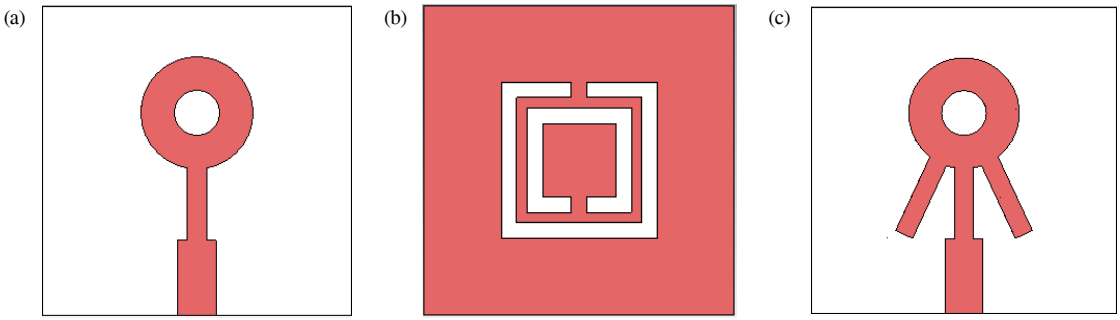

FIGURE 1. Design stages, (a) stage 1, (b) stage 2, (c) stage 3.

23.41 and 45 GHz are proposed in [25, 26]. Designs for high bandwidth incorporate multiple resonators [27] and multi-band operation is achieved using metamaterial and monopole configurations [28]. A dual-band patch for portable 5G devices operates at 28/38 GHz [29]. Other innovations include donut-shaped patches for enhanced gain at 28 GHz [30] and flexible antennas for IoT, wearable devices, robotics, and healthcare [31–34]. Specific designs are presented for wearable applications, featuring highly flexible patches operating at 28.9–31.75 GHz, capable of data rates up to 1 Gbps over 70–100 m in [35]. Moreover, the mmWave spectrum, offering wide bandwidth and low latency, is a promising solution for medical applications [36]. A triple-band coplanar waveguide (CPW) monopole antenna designed for IoT was presented in [37], achieving bandwidths of 22–30 GHz, 37–39 GHz, and 56.5–61 GHz, with gains of 5.29, 7.49, and 9 dBi and a SAR value in the range of 0.9–0.62 W/kg. Another design in [38] featured a triple-band antenna for IoT applications by combining two monopoles of varying lengths with a conducting stub at the base. This design achieved bandwidths of 445 MHz, 657 MHz, and 5.14 GHz at 3.5 GHz, 5.8 GHz, and 28 GHz, respectively, with corresponding antenna gains of 1.86, 2.55, and 4.41 dBi.

However, due to the rigid properties of the materials used, these antenna designs have several drawbacks, such as a bigger overall size, less bandwidth, reduced gain, more back radiation, and limited medical suitability. Additionally, this study's use of semi-flexible RT/duroid 3003 material has effectively addressed the issues associated with the rigidity and inflexibility of conventional antennas [39]. The wearable mmWave antenna that operates across dual frequency bands is a significant research field, according to the aforementioned studies. Thus, the wearable mmWave antenna is designed in the proposed work.

The key contributions of this study are summarized as follows:

(a) The development of a dual-band patch antenna operating at 28 GHz and 38 GHz, tailored for 5G applications.

(b) The antenna features a low-profile structure and is fabricated on a flexible Rogers 3003 substrate, making it ideal for wearable applications and integration into compact devices.

(c) Bending investigation in mmWave frequencies: The antenna's performance is tested in both flat and bent configurations, demonstrating its flexibility and suitability for wearable technologies.

(d) SAR analysis in mmWave frequencies: The study includes a comprehensive evaluation of SAR values, ensuring the antenna's safety for wearable and biomedical applications.

2. ANTENNA DESIGN AND EVOLUTION

2.1. Structure and Dimensions

Primarily the fundamental microstrip-fed antenna is used to establish the design criteria for the antenna. The patch's measurements, such as its length and width, are then calculated using the transmission line model as described in [40]. The Computer Simulation Technology Microwave Studio (CST MWS)®software is used for evaluating changes that affect the radiating plane's surrounding sizes and optimize parameters. An RT/duroid 3003 semi-flexible material ($\varepsilon r = 3$, $\tan\delta = 0.0013$) with the thickness of 1.52 mm was used as a substrate. The proposed antenna design is developed in multiple stages, with the corresponding figures illustrated in Fig. 1. In Stage 1, a circular radiating patch is placed on the top of the substrate with a full ground plane, as depicted in Fig. 1(a). This initial antenna is designed to resonate at 28 GHz. In Stage 2, a square split ring resonator is incorporated into the ground plane to introduce a second resonant frequency at 38 GHz, as shown in Fig. 1(b). Finally, to achieve optimal impedance matching and enhance the bandwidth, a "round necktie" configuration is implemented by adding two diagonal rectangular patches to the periphery of the radiating patch, as illustrated in Fig. 1(c).

This final design effectively operates at the targeted frequencies of 28 GHz and 38 GHz, making it suitable for 5G mmWave applications. The finalized antenna geometry is presented in Fig. 2. A total dimension of $15 \times 15 \times 1.52\,\text{mm}^3$ was selected. A comparison of the simulated reflection coefficient (S_{11}) at various design stages is shown in Fig. 3.

2.2. Parametric Analysis

To evaluate the impact of design modifications on the antenna's performance, a comprehensive investigation was conducted, including a parametric study focusing on critical parameters such

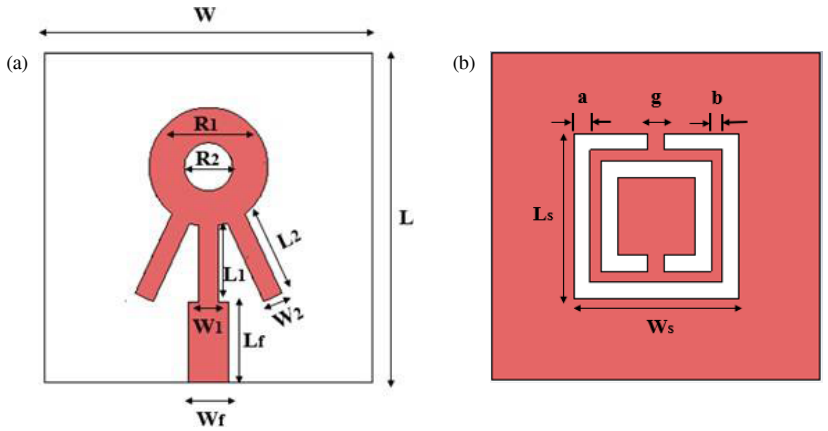

FIGURE 2. Proposed antenna, (a) front, (b) back. Antennas dimensions are $L = 15\,\text{mm}$, $W = 15\,\text{mm}$, $R1 = 5.4\,\text{mm}$, $R2 = 2.2\,\text{mm}$, $W1 = 1\,\text{mm}$, $L1 = 3.4\,\text{mm}$, $W2 = 1\,\text{mm}$, $L2 = 4\,\text{mm}$, $Wf = 1.8\,\text{mm}$, $Lf = 3.7\,\text{mm}$, $Ls = 7.6\,\text{mm}$, $Ws = 7.6\,\text{mm}$, $g = 0.75\,\text{mm}$, $a = 1\,\text{mm}$, $b = 0.7\,\text{mm}$.

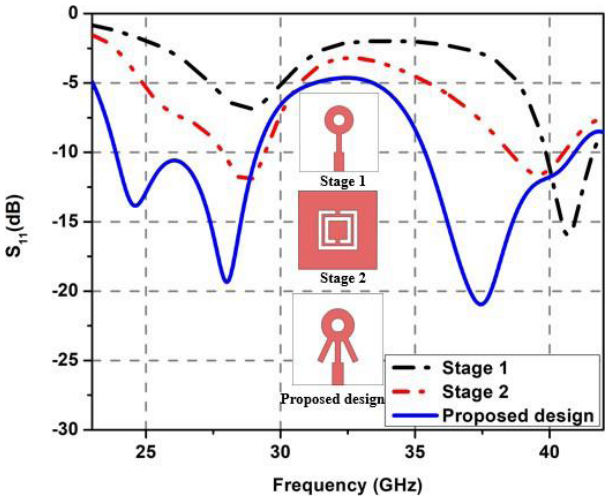

FIGURE 3. S_{11} comparison of the proposed antenna at various design stages.

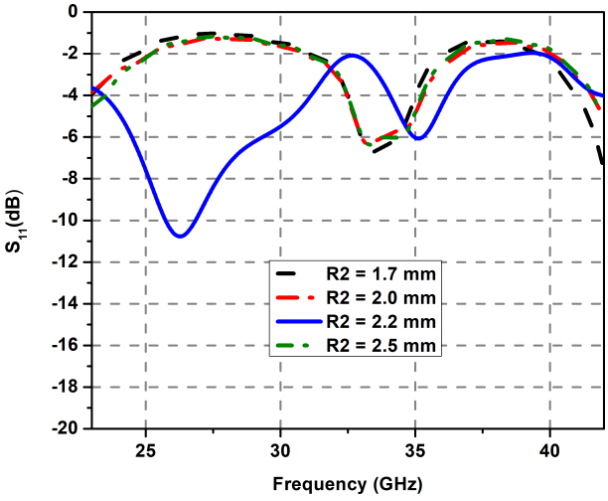

FIGURE 4. S_{11} changes with $R2$.

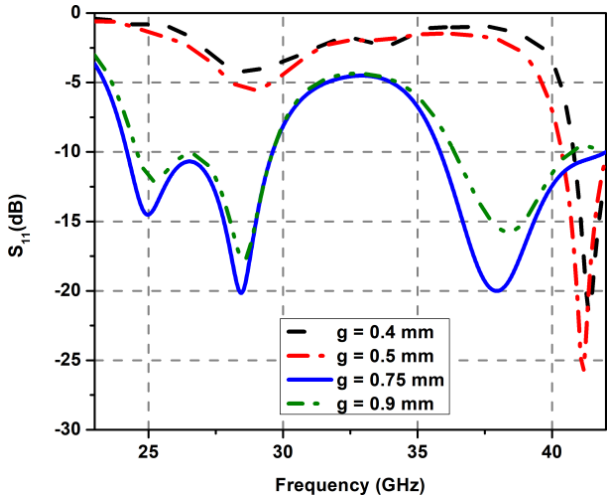

FIGURE 5. S_{11} changes with g.

as $R2$, g, a, and $L2$. The goal of this analysis was to identify the optimal values for these parameters to enable precise tuning of the antenna design. This tuning aimed to enhance the antenna's efficiency, broaden its frequency range, and improve signal reception for mmWave applications. The study began by optimizing the inner radius ($R2$) of the circular patch within the range of 1.7 mm to 2.5 mm. An optimal value of 2.2 mm was identified, providing superior coverage of the target mmWave frequency bands and contributing to improved signal reception and performance as seen in Fig. 4. For the gap (g) in the square split-ring resonator, which affects the 38 GHz frequency band (Fig. 5), the parameter was varied from 0.4 mm to 0.9 mm. The study found that an optimal gap of 0.75 mm achieved the best coverage for the 38 GHz frequency band, thus optimizing the antenna design for improved efficiency and broader frequency coverage. Additionally, the slot (a) in the square split-ring resonator, shown in Fig. 6 was optimized within the range of 0.7 mm to 1.2 mm. The optimal slot length of 1.0 mm was determined, enhancing the overall performance of the antenna for mmWave applications. Finally, the effect of $L2$ on antenna performance was analyzed, as presented in Fig. 7. The parameter $L2$ was varied from 1.0 mm to 5.0 mm, with an optimal value of 4.0 mm found to maximize antenna performance. This detailed parametric study highlights the critical dimensions influencing the antenna's performance, enabling precise tuning to achieve improved efficiency, wider frequency coverage, and enhanced signal reception for mmWave applications.

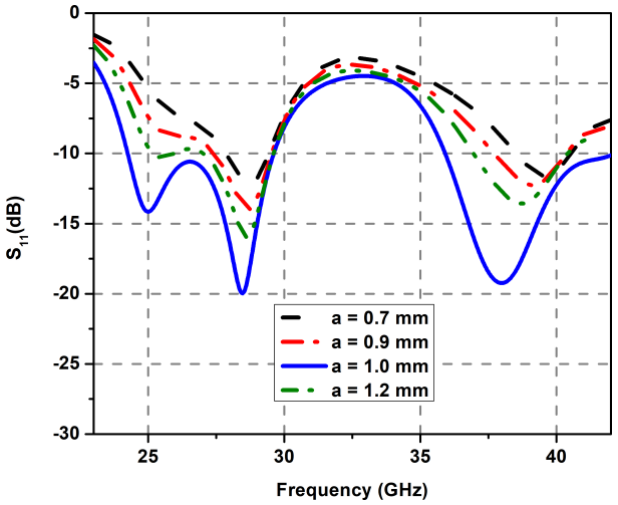

FIGURE 6. S_{11} changes with a.

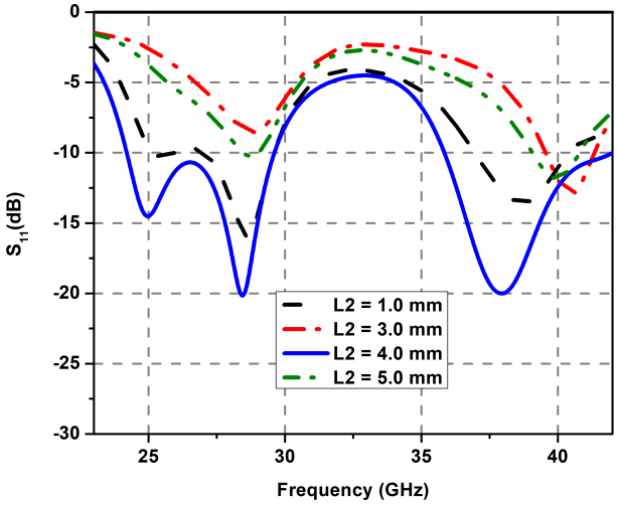

FIGURE 7. S_{11} changes with $L2$.

3. RESULTS AND ANALYSIS

The fabricated antenna was utilized to validate the proposed design, as shown in Fig. 8. The S_{11} was evaluated through both simulation and measurement with the results seen in Fig. 9. Measurements revealed enhanced performance in the first resonant band, attributed to its inherently stronger response. Slight variations in the measured results can be linked to the very thin feedline, which might have resulted in minor misalignment during the soldering process. Nevertheless, the resonance frequencies in both the measured and simulated results align closely. This confirms that the antenna operates in dual-band mode, resonating at both 28 GHz and 38 GHz. The current distribution of the proposed antenna is depicted in Fig. 10. At 28 GHz, the current is primarily concentrated around the circular slots, suggesting that these slots play a key role in generating the 28 GHz resonance. Conversely, at the higher resonant frequency of 38 GHz, the maximum current is localized near the square split-ring resonator (SSRR). Fig. 11 illustrates the measured and simulated radiation patterns. At 38 GHz, the measured patterns demonstrate omnidirectional behavior in the H-plane and directional behavior in the E-plane, closely matching the simulated outcomes in Fig. 11(a). A small deviation, how-

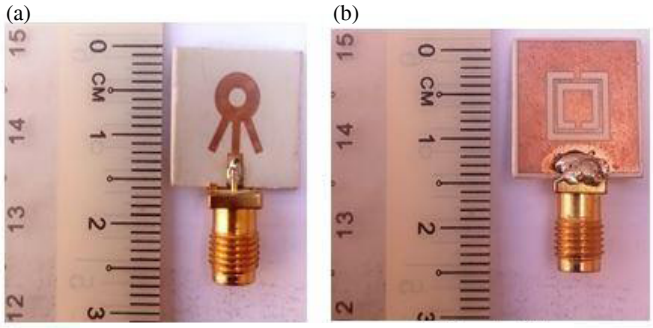

FIGURE 8. Prototype antenna. (a) Front side. (b) Back side.

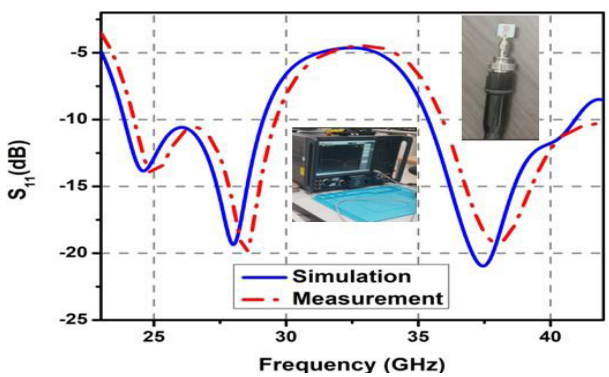

FIGURE 9. S_{11} comparison.

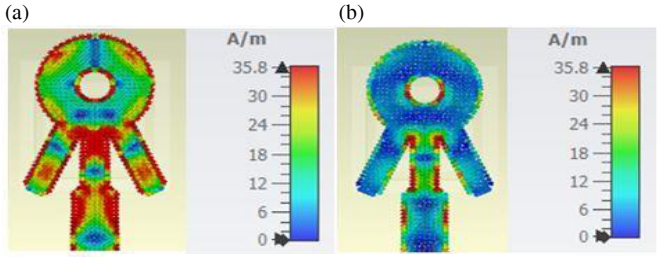

FIGURE 10. Current distributions of the proposed antenna. (a) 28 GHz, (b) 38 GHz.

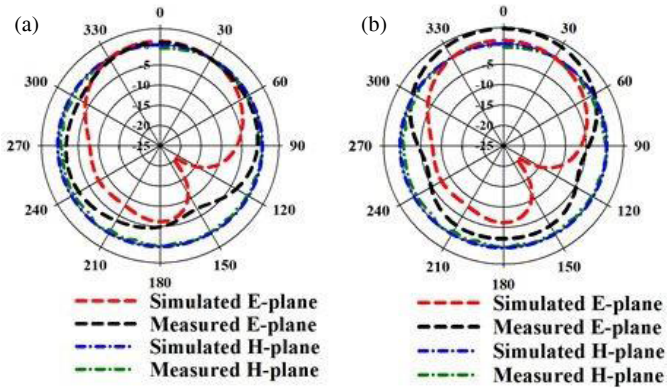

FIGURE 11. Radiation patterns of the proposed antenna. (a) 28 GHz, (b) 38 GHz.

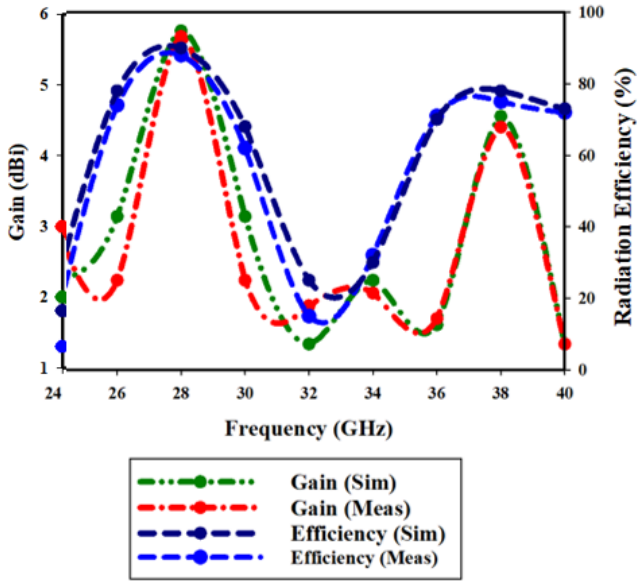

FIGURE 12. Gain vs efficiency of the proposed antenna.

ever, is seen in the measured patterns at 38 GHz relative to the simulation in Fig. 11(b), potentially caused by cable losses.

The antenna achieves a measured gain of 5.91 dBi at 28 GHz and 4.57 dBi at 38 GHz, with corresponding efficiencies of 90% and 78%, respectively, as illustrated in Fig. 12. These findings indicate that the antenna maintains consistent gain for signal transmission and reception across its operational bandwidth, highlighting its suitability for 5G and wearable applications.

4. BENDING ANALYSIS

Wearable antennas are made to adapt to the surface of the human body and tolerate bending while in use in a variety of applications. This demands assessing how well they function under bending situations, especially in medical applications. In order to guarantee reliable performance, it is essential to investigate their behaviour under various bending configurations in an unhindered condition prior to analyzing the effects of body tissue loading. Two orientations were examined, specifically along the x- and y-axes. Fig. 13 depicts bending along the x-axis at diameters (d) of 50 mm, 70 mm, 90 mm, and 110 mm. Fig. 14 displays the matching S_{11} graphs. As the diameter increases, these figures show a tiny upward shift in the matching of the S_{11} at the upper resonant frequency of 38 GHz. Fig. 15 shows the realized gain at various bending diameters along the x-axis. It shows that the antenna's peak realized gain is approximately 5.25 dBi and stays relatively constant at both working bands. Similarly, the y-axis bending analysis for different diameters is presented in Fig. 16. With increasing bending diameter, both resonant frequencies experience a slight upward shift, accompanied by improved antenna matching, as illustrated in Fig. 17. Additionally, the peak realized gain of the bent antenna at 28 GHz and 38 GHz shows a minor upward shift, as depicted in Fig. 18. This study demonstrates that the resonance and gain of the antenna remain consistent across different bending orientations and diameters, making it suitable for wearable electronics, IoT, and biomedical applications.

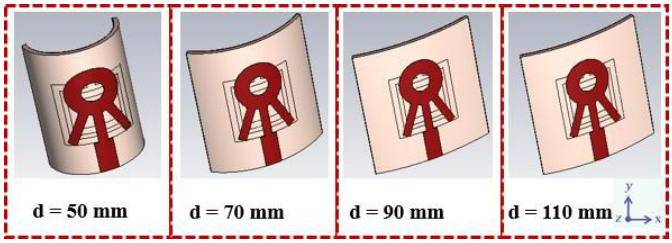

FIGURE 13. Proposed antenna under bending in the x-axis.

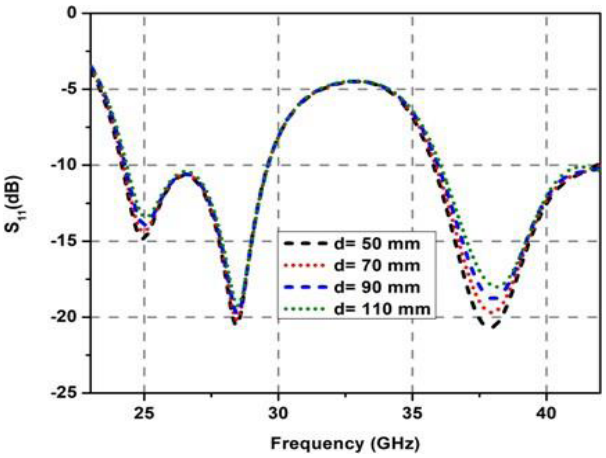

FIGURE 14. S_{11} under bending conditions in the x-axis.

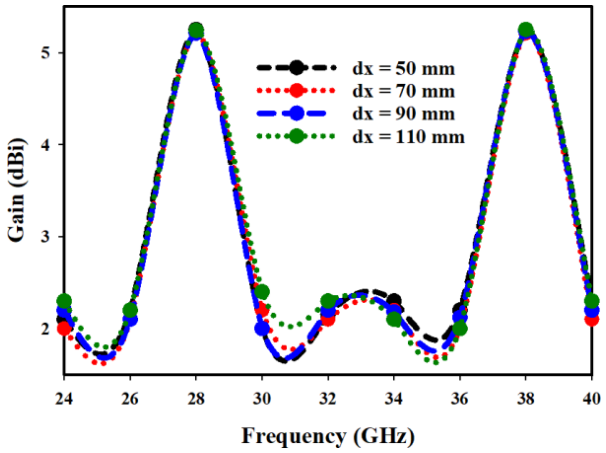

FIGURE 15. Gain under bending in the x-axis.

5. SAR INVESTIGATION

Wearable antennas must account for SAR values because of their direct exposure to the human body. Compliance with regulatory standards, such as those set by the FCC and ICNIRP, is essential, with maximum thresholds defined as 1.6 W/kg for 1 g of tissue and 2 W/kg for 10 g of tissue [41, 42]. The SAR values are computed in CST MWS®software following the IEEE C95.1 standard. A four-layer human body tissue model comprising skin, fat, muscle, and bone is utilized for these simulations, as illustrated in Fig. 19. The material properties of these tissue layers are adopted from [41].

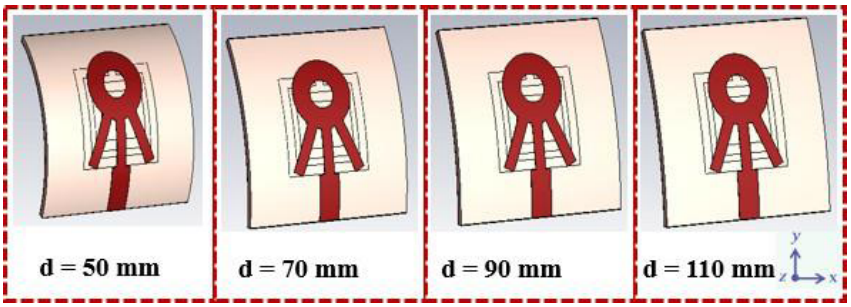

FIGURE 16. Proposed antenna under bending in the y-axis.

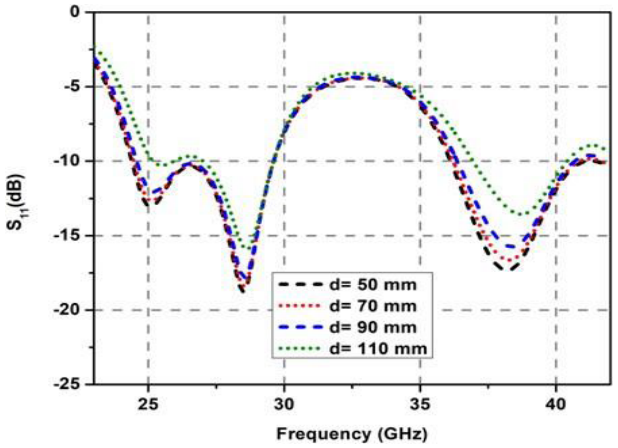

FIGURE 17. S_{11} under bending conditions in the y-axis.

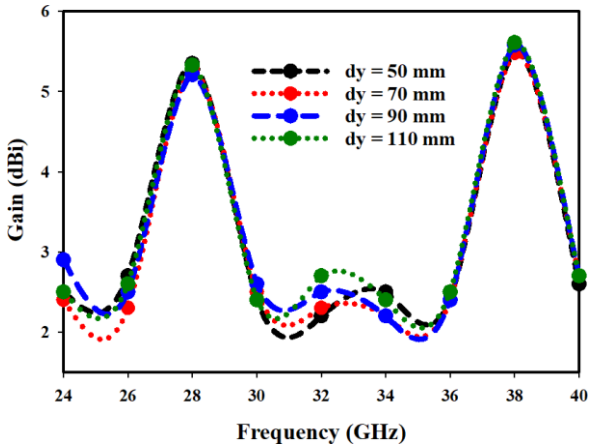

FIGURE 18. Gain under bending in the y-axis.

TABLE 1. SAR values for 1/10 g for varying incident power.

Power (mW)	50		100		150		200	
Mass of human tissue (g)	1	10	1	10	1	10	1	10
Frequency (GHz)	SAR values (W/kg)							
28	0.22	0.27	0.37	0.29	0.57	0.31	0.69	0.77
38	0.06	0.04	0.09	0.05	0.18	0.16	0.25	0.31

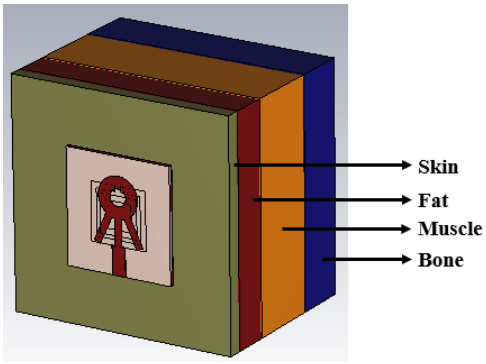

FIGURE 19. Human body tissue model.

To evaluate SAR values, input power levels ranging from 50 to 200 mW were applied. Table 1 presents the simulated SAR values for 1 g and 10 g of human tissue at 28 GHz and 38 GHz under different input power levels. The table shows a decrease in SAR values at higher frequencies, likely due to the dielectric properties of human tissues. The SAR values of the antenna are depicted in Figs. 20 and 21. At 28 GHz and an input power of 150 mW, the SAR values for 1 g and 10 g of human tissue are 0.57 W/kg and 0.31 W/kg, respectively, as seen in Figs. 20(a) and 20(b). At 38 GHz, the SAR values are 0.18 W/kg and 0.16 W/kg, as shown in Figs. 21(a) and 21(b). These results demonstrate that the antenna's SAR values meet the safety standards set by the FCC and ICNIRP.

Table 2 presents a comparative analysis of the proposed antenna's performance against existing designs. The developed antenna exhibits notably more compact dimensions than most counterparts listed in the table. Analysis reveals that its physical size is markedly reduced relative to earlier implementations. Furthermore, the design achieves satisfactory operational metrics including bandwidth, SAR values, gain, and efficiency at

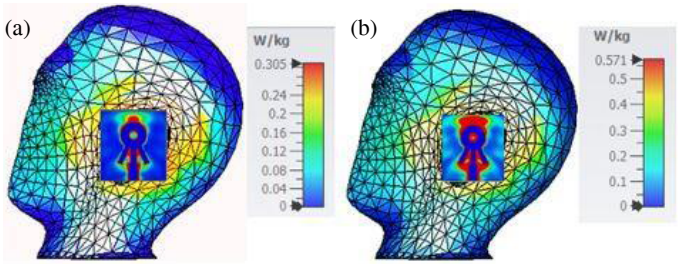

FIGURE 20. SAR values with human body tissue model at 28 GHz (a) 1 g (b) 10 g.

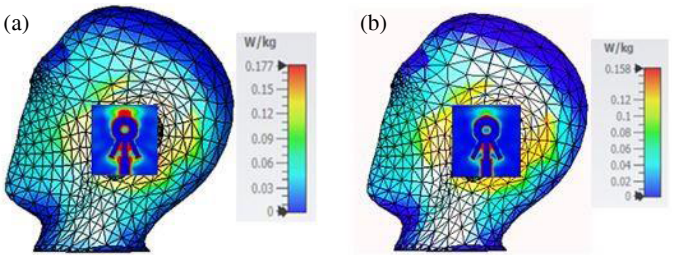

FIGURE 21. SAR values with human body tissue model at 38 GHz (a) 1 g (b) 10 g.

TABLE 2. Comparison of the proposed antenna performance with that of earlier research.

Ref.	Dimension (mm^2)	Frequency (GHz)	Substrate Material	Bandwidth (%)	Gain (dBi)	SAR (W/kg)	Efficiency (%)
[2]	$12 \times 3 \times 0.25$	28/38	Rogers	2.4/2.26	5.36/5.5	0.91/1.36	70/71
[22]	$6 \times 6 \times 0.25$	26/28	Rogers	5.9/6.6	7.4/7.9	0.063/0.0206	NA
[29]	$14 \times 12 \times 0.38$	28/38	Rogers	9.1/5.52	1.27/1.83	NA	78/76
[31]	$19.5 \times 21.8 \times 2$	25/38	Cotton	12/4.9	4/3.5	NA	37/49
[37]	$4 \times 3 \times 0.25$	27/38	Rogers	29/3.9	5.29/7.49	0.9/0.62	65/70
[43]	$25 \times 15 \times 0.5$	28/38	Taconic	3.8/9	8.4/6.1	NA	84/99
[44]	$12 \times 12 \times 0.25$	28/40	Rogers	28/7.5	4.9/4.2	NA	82/85
This work	$15 \times 15 \times 1.52$	**28/38**	**Rogers**	**21.4/23.7**	**5.91/4.57**	**0.57/0.18**	**90/78**

target resonant frequencies. The data in Table 2 underscores the antenna's superiority over prior designs, highlighting its enhanced performance across multiple parameters.

6. CONCLUSION

This study introduces a compact dual-band wearable antenna tailored for mmWave applications. Fabricated on a Rogers 3003 dielectric substrate, the antenna measures $15 \times 15 \times 1.52\,mm^3$. Its design features a circular radiating patch on the top layer and a full ground plane on the bottom. While initially designed for single-band operation at 28 GHz, the integration of an SSRR into the ground plane enabled dual-band resonance, achieving an additional operational frequency at 38 GHz. To enhance bandwidth and gain, two rectangular patches were diagonally positioned along the radiating element, forming a bowtie-inspired configuration. Experimental results reveal impedance bandwidths of 21.4% and 23.7% at 28 GHz and 38 GHz, respectively. The antenna exhibits peak gains of 5.91 dBi and 4.57 dBi with radiation efficiencies of 90% and 78% in the respective bands. Simulated SAR values for 1 g and 10 g tissue samples remain well below regulatory thresholds (0.57/0.31 W/kg at 28 GHz; 0.18/0.16 W/kg at 38 GHz), complying with FCC and ICNIRP safety guidelines. Bending tests confirm the antenna's stable performance under deformation, underscoring its robustness for wearable use. It has compact size, dual-band operation, and compliance with safety standards, positioning the antenna as a viable solution for 5G systems and biomedical wearable technologies.

ACKNOWLEDGEMENT

This work is partially supported by the UK Engineering and Physical Sciences Research Council (EPSRC) under grant EP/Y035135/1, and HORIZON-MSCA-2022-SE-01-01-ID: 101131501, Marie Skłodowska-Curie, Research and Innovation Staff Exchange (RISE), titled: titled: 6G Terahertz Communications for Future Heterogeneous Wireless Network (6G-TERAFIT). In addition, the Nigerian government Scholarship fund has sponsored the studentship of Mr Abubakar Salisu.

REFERENCES

[1] Shariff, B. G. P., T. Ali, P. R. Mane, M. G. N. Alsath, P. Kumar, S. Pathan, A. A. Kishk, and T. Khan, "Design and measurement of a compact millimeter wave highly flexible MIMO antenna loaded with metamaterial reflective surface for wearable applications," *IEEE Access*, Vol. 12, 30 066–30 084, 2024.

[2] Tiwari, R. N., O. S. Sai, D. Sharma, M. S. Kumar, P. Singh, P. Kumar, C. Sreemanya, and S. Rajasekaran, "A low-profile dual-band millimeter wave patch antenna for high-speed wearable and biomedical applications," *Results in Engineering*, Vol. 24, 103212, 2024.

[3] Pons, M., E. Valenzuela, B. Rodríguez, J. A. Nolazco-Flores, and C. Del-Valle-Soto, "Utilization of 5G technologies in IoT applications: Current limitations by interference and network optimization difficulties — A review," *Sensors*, Vol. 23, No. 8, 3876, 2023.

[4] Mukherjee, K., S. Mukhopadhyay, and S. Roy, "Design of a wideband Y-shaped antenna for the application in IoT and 5G

communication," *International Journal of Communication Systems*, Vol. 35, No. 1, e5021, 2022.

[5] Zada, M., I. A. Shah, and H. Yoo, "Integration of sub-6-GHz and mm-wave bands with a large frequency ratio for future 5G MIMO applications," *IEEE Access*, Vol. 9, 11 241–11 251, 2021.

[6] Uwaechia, A. N. and N. M. Mahyuddin, "A comprehensive survey on millimeter wave communications for fifth-generation wireless networks: Feasibility and challenges," *IEEE Access*, Vol. 8, 62 367–62 414, 2020.

[7] Jiang, S., R. Song, Z. Hu, Y. Xin, G.-L. Huang, and D. He, "Millimeter wave phased array antenna based on highly conductive graphene-assembled film for 5G applications," *Carbon*, Vol. 196, 493–498, 2022.

[8] Abbasi, N. A., B. Virdee, I. U. Din, S. Ullah, A. A. Althuwayb, N. Rashid, M. Soruri, C. H. See, and M. Alibakhshikenari, "High-isolation array antenna design for 5G mm-Wave MIMO applications," *Journal of Infrared, Millimeter, and Terahertz Waves*, Vol. 46, No. 1, 12, 2025.

[9] Hong, T., S. Zheng, R. Liu, and W. Zhao, "Design of mmWave directional antenna for enhanced 5G broadcasting coverage," *Sensors*, Vol. 21, No. 3, 746, 2021.

[10] Jemaludin, N. H. B., A. J. A. Al-Gburi, R. H. Elabd, T. Saeidi, M. F. Akbar, I. M. Ibrahim, and Z. Zakaria, "A comprehensive review on MIMO antennas for 5G smartphones: Mutual coupling techniques, comparative studies, SAR analysis, and future directions," *Results in Engineering*, Vol. 23, 102712, 2024.

[11] Du, Y., Y. Wang, Y. Yan, W. Yan, P. Xu, X. Xu, D. Wang, N. Zong, M. Wang, and C. Wang, "Reconfigurability enhancement of pixel array antennas based on WOA and MPUC," *AEU — International Journal of Electronics and Communications*, Vol. 178, 155240, 2024.

[12] Musa, U., S. M. Shah, H. A. Majid, Z. Z. Abidin, M. S. Yahya, S. Babani, and Z. Yunusa, "Recent advancement of wearable reconfigurable antenna technologies: A review," *IEEE Access*, Vol. 10, 121 831–121 863, 2022.

[13] Ashyap, A. Y. I., S. H. B. Dahlan, Z. Z. Abidin, S. K. A. Rahim, H. A. Majid, A. S. M. Alqadami, and M. E. Atrash, "Fully fabric high impedance surface-enabled antenna for wearable medical applications," *IEEE Access*, Vol. 9, 6948–6960, 2021.

[14] Hussain, S., S. Hafeez, S. A. Memon, and N. Pirzada, "Design of wearable patch antenna for wireless body area networks," *(IJACSA) International Journal of Advanced Computer Science and Applications*, Vol. 9, No. 9, 146–151, 2018.

[15] Basir, A., A. Bouazizi, M. Zada, A. Iqbal, S. Ullah, and U. Naeem, "A dual-band implantable antenna with wide-band characteristics at MICS and ISM bands," *Microwave and Optical Technology Letters*, Vol. 60, No. 12, 2944–2949, 2018.

[16] Bahrouni, M., G. Houzet, T. P. Vuong, P. M. Mendes, H. Dinis, R. Silva, and H. Trabelsi, "Modeling of a compact, implantable, dual-band antenna for biomedical applications," *Electronics*, Vol. 12, No. 6, 1475, 2023.

[17] Salama, S., D. Zyoud, and A. Abuelhaija, "Design of a dual-band planar inverted FL implantable antenna for biomedical applications," in *Journal of Physics: Conference Series*, Vol. 1711, No. 1, 012002, 2020.

[18] Savcı, H. and F. Kaburcuk, "FDTD-based SAR calculation of a wearable antenna for wireless body area network devices," *International Journal of Microwave and Wireless Technologies*, Vol. 15, No. 8, 1354–1360, 2023.

[19] Savcı, H., H. Sajjad, S. Khan, and F. Kaburcuk, "Analysis of a compact multi-band textile antenna for WBAN and WLAN applications," *Balkan Journal of Electrical and Computer Engineering*, Vol. 9, No. 3, 255–260, 2021.

[20] Wu, R., J. Dong, and M. Wang, "Wearable polarization conversion metasurface MIMO antenna for biomedical applications in 5 GHz WBAN," *Biosensors*, Vol. 13, No. 1, 73, 2023.

[21] Michel, A., R. Colella, G. A. Casula, P. Nepa, L. Catarinucci, G. Montisci, G. Mazzarella, and G. Manara, "Design considerations on the placement of a wearable UHF-RFID PIFA on a compact ground plane," *IEEE Transactions on Antennas and Propagation*, Vol. 66, No. 6, 3142–3147, 2018.

[22] Bhadrvathi Ghouse, P. S., P. R. Mane, S. T. Sumangala, V. K. Puttur, S. Pathan, V. K. Jhunjhunwala, and T. Ali, "A compact dual-band millimeter wave antenna for smartwatch and IoT applications with link budget estimation," *Sensors*, Vol. 24, No. 1, 103, 2023.

[23] Han, C.-Z., G.-L. Huang, T. Yuan, and C.-Y.-D. Sim, "A dual-band millimeter-wave antenna for 5G mobile applications," in *2019 IEEE International Symposium on Antennas and Propagation and USNC-URSI Radio Science Meeting*, 1083–1084, 2019.

[24] Farooq, U. and G. M. Rather, "A miniaturised Ka/V dual band millimeter wave antenna for 5G body centric network applications," *Alexandria Engineering Journal*, Vol. 61, No. 10, 8089–8096, 2022.

[25] Ullah, H. and F. A. Tahir, "A high gain and wideband narrow-beam antenna for 5G millimeter-wave applications," *IEEE Access*, Vol. 8, 29 430–29 434, 2020.

[26] Khattak, M. I., A. Sohail, U. Khan, Z. Barki, and G. Witjaksono, "Elliptical slot circular patch antenna array with dual band behaviour for future 5G mobile communication networks," *Progress In Electromagnetics Research C*, Vol. 89, 133–147, 2019.

[27] Bembarka, A., L. Setti, A. Tribak, H. Tizyi, and M. E. Ouahabi, "A novel wideband beamforming antenna for 5G applications by eliminating the phase shifters and crossovers from the Butler matrix," *Progress In Electromagnetics Research C*, Vol. 133, 51–63, 2023.

[28] Siyara, J. P., M. N. Jiyani, O. Alsalman, S. P. Lavadiya, and S. K. Patel, "Novel metamaterial array-based dual port MIMO antenna using low profile substrate with feature multiband, and high isolation for sub-6G, IoT, and WiMAX applications," *Physica Scripta*, Vol. 99, No. 9, 095531, Aug. 2024.

[29] Hasan, M. N., S. Bashir, and S. Chu, "Dual band omnidirectional millimeter wave antenna for 5G communications," *Journal of Electromagnetic Waves and Applications*, Vol. 33, No. 12, 1581–1590, 2019.

[30] Kamal, M. M., S. Yang, S. H. Kiani, M. R. Anjum, M. Alibakhshikenari, Z. A. Arain, A. A. Jamali, A. Lalbakhsh, and E. Limiti, "Donut-shaped mmwave printed antenna array for 5G technology," *Electronics*, Vol. 10, No. 12, 1415, 2021.

[31] Mallat, N. K., A. Jafarieh, H. Noorollahi, and M. Nouri, "A novel fractal arrow-shaped mmWave flexible antenna for IoT and 5G communication systems," *Progress In Electromagnetics Research Letters*, Vol. 107, 9–17, 2022.

[32] Didi, S.-E., I. Halkhams, A. Es-saqy, M. Fattah, S. Mazer, and M. E. Bekkali, "Creation of a soft circular patch antenna for biomedical applications for 5G at frequency 2.45 GHz," *Results in Engineering*, Vol. 22, 102319, 2024.

[33] Wagih, M., G. S. Hilton, A. S. Weddell, and S. Beeby, "Broadband millimeter-wave textile-based flexible rectenna for wearable energy harvesting," *IEEE Transactions on Microwave Theory and Techniques*, Vol. 68, No. 11, 4960–4972, 2020.

[34] Al-Alem, Y., S. M. Sifat, Y. M. M. Antar, and A. A. Kishk, "Millimeter-wave planar antenna array augmented with a low-cost 3D printed dielectric polarizer for sensing and internet of things (IoT) applications," *Scientific Reports*, Vol. 13, No. 1,

9646, 2023.

[35] Shariff, B. G. P., S. Pathan, P. R. Mane, and T. Ali, "Characteristic mode analysis based highly flexible antenna for millimeter wave wireless applications," *Journal of Infrared, Millimeter, and Terahertz Waves*, Vol. 45, No. 1, 1–26, 2024.

[36] Mallat, N. K., M. Ishtiaq, A. U. Rehman, and A. Iqbal, "Millimeter-wave in the face of 5G communication potential applications," *IETE Journal of Research*, Vol. 68, No. 4, 2522–2530, 2022.

[37] Ahmad, S., H. Boubakar, S. Naseer, M. E. Alim, Y. A. Sheikh, A. Ghaffar, A. J. A. Al-Gburi, and N. O. Parchin, "Design of a tri-band wearable antenna for millimeter-wave 5G applications," *Sensors*, Vol. 22, No. 20, 8012, 2022.

[38] Ruchi, R., A. Patnaik, and M. V. Kartikeyan, "Compact dual and triple band antennas for 5G-IOT applications," *International Journal of Microwave and Wireless Technologies*, Vol. 14, No. 1, 115–122, 2022.

[39] Balanis, C. A., *Modern Antenna Handbook*, John Wiley & Sons, 2011.

[40] Hirtenfelder, F., "Effective antenna simulations using CST MICROWAVE STUDIO®," in *2007 2nd International ITG Conference on Antennas*, 239–239, Munich, Germany, Mar. 2007.

[41] Musa, U., S. M. Shah, H. B. A. Majid, M. K. A. Rahim, M. S. Yahya, Z. Yunusa, A. Salisu, and Z. Z. Abidin, "Wearable dual-band frequency reconfigurable patch antenna for WBAN applications," *Progress In Electromagnetics Research M*, Vol. 120, 95–111, 2023.

[42] Musa, U., S. M. Shah, H. A. Majid, I. A. Mahadi, K. A. R. Mohamad, M. S. Yahya, and Z. Z. Abidin, "Investigation of the nonlinearity of PIN diode on frequency reconfigurable patch antenna," *The Journal of Engineering*, Vol. 2023, No. 9, e12308, 2023.

[43] Liu, P., X.-W. Zhu, Y. Zhang, X. Wang, C. Yang, and Z. H. Jiang, "Patch antenna loaded with paired shorting pins and H-shaped slot for 28/38 GHz dual-band MIMO applications," *IEEE Access*, Vol. 8, 23 705–23 712, 2020.

[44] Munir, M. E., S. H. Kiani, H. S. Savci, M. Marey, J. Khan, H. Mostafa, and N. O. Parchin, "A four element mm-wave MIMO antenna system with wide-band and high isolation characteristics for 5G applications," *Micromachines*, Vol. 14, No. 4, 776, 2023.